Remote influence on regional scale intraseasonal rainfall variability over Vietnam

Hong-Hanh Le, Nicholas M. J. Hall, Thanh Ngo-Duc

Received: 29 March 2023 | Revised: 27 November 2023 | Accepted: 13 January 2024

DOI: 10.1002/joc.8377

RESEARCH ARTICLE

International Journal of Climatology RMetS

Remote influence on regional scale intraseasonal rainfall variability over Vietnam

Hong-Hanh Le[1] | **Nicholas M. J. Hall**[1] | **Thanh Ngo-Duc**[2]

[1]LEGOS/University of Toulouse: UT3/IRD/CNRS/CNES, Toulouse, France

[2]LOTUS, Department of Space and Applications, University of Science and Technology of Hanoi, Vietnam Academy of Science and Technology, Hanoi, Vietnam

Correspondence
Hong-Hanh Le, LEGOS/University of Toulouse: UT3/IRD/CNRS/CNES, Toulouse, France.
Email: lehonghanh.lhh@gmail.com

Funding information
Ministére de l'Education Nationale, de l'Enseignement Superieur et de la Recherche

Abstract

Remote influences on intraseasonal anomalous rainfall over regions that encompass North and South Vietnam are explored using a 38-year (1979–2016) global dataset over the extended summer (May–October). Wet and Dry composites in filtered daily data with lags of up to 2 weeks are assembled for various rainfall indices over the two subregions, including atmospheric reanalysis products and in-situ rainfall data. On the regional scale, the moisture flux convergence correlates well with reanalysed rainfall. The large-scale dynamics associated with these composites are described. Rainfall composites of opposing signs show asymmetrical large-scale precursors and different pathways of influence. Wet and Dry anomalies in North Vietnam are seen to originate from Europe and propagate at high latitudes. The exact nature of the precursors is sensitive to the definition of the composite index. There is also a pathway of influence along the Asian jet, which impacts South Vietnam, especially for Wet composites which often coincide with Dry conditions in the North. South Vietnam is also influenced by tropical divergent precursors, which are again asymmetric between Wet and Dry composites.

KEYWORDS

anomalous rainfall, intraseasonal variability (ISV), large-scale dynamics, remote influences, tropical waves

1 | INTRODUCTION

The annual cycle of rainfall over Vietnam is controlled by the seasonal Southeast Asia monsoon system. However, within a season there are large variations that account for a major fraction of the total rainfall variability (Yokoi et al., 2007). Intraseasonal anomalies during the rainy season from May to October can take the form of prolonged periods of flood or drought or extreme events of shorter duration, for example, Wu et al. (2012); Linden, Fink, Phan-Van, and Trinh-Tuan (2016). Such anomalous rainfall can have important consequences for agriculture and water resources. This study focuses on remote influences on rainfall anomalies over Vietnam on regional spatial scales and intraseasonal time scales.

Intraseasonal variations (ISV) of rainfall over Vietnam have previously been characterised as spatio–temporal modes. Yokoi and Satomura (2005) and Yokoi et al. (2007) used a wavelet analysis of daily rain gauge data over the Indochina Peninsula and identified two ISV timescales for different horizontal distributions of rainfall over Vietnam. They showed that a 30–60 day variation is observed in

Central Vietnam in July–October, while a 10–20 day variation is observed in North and Central Vietnam in May–September. Truong and Tuan (2018)—TT18 and Truong and Tuan (2019)—TT19, also showed that daily rainfall from selected stations in Vietnam displays significant variability on 30–60 day and 10–20 day time scales.

There have been relatively few investigations that discriminate between wet and dry anomalies over Vietnam subregions on intraseasonal timescales. The problem is sensitive to the choice of region, timescale, dataset, and analysis technique.

For example, Tuan (2019) used principal component (PC) analysis to extract spatial patterns of sub-monthly rainfall variation using high-resolution gridded precipitation data from 1980 to 2010 over Vietnam (Nguyen-Xuan et al., 2016) with a time filter of 7–25 day. Four patterns were identified, each of which covers the entire region. Only the active (Wet) phases of PCs were considered. On the other hand, TT18 and TT19 concentrated on individual regions and isolated time periods of 10–20 day and 20–60 day respectively, using station data, which is mostly concentrated along the coast. They consider wet and dry phases as part of a cycle. Other investigators have looked at individual wet cases over Vietnam subregions, for example, Linden, Fink, Phan-Van, and Trinh-Tuan (2016), Yokoi and Matsumoto (2008), Wu et al. (2012).

Given the multiplicity of regions, rainfall criteria, and timescales to consider, it is worthwhile investigating explicitly the sensitivity of the conclusions to such considerations at the regional scale. In this study, we diagnose remote influences separately for wet and dry composites and pay particular attention to their interrelations across relatively large regions. We will use vertically integrated moisture flux convergence (VIMC) as a proxy for rainfall ISV since it is highly correlated with regional-scale rainfall. VIMC is a quantity that is close to the large-scale dynamics and is available from a consistent dataset.

We consider two types of remote influence: tropical and extratropical. Tropical phenomena such as the Madden Julian Oscillation (MJO) (Madden & Julian, 1972), and equatorial Rossby and Kelvin waves are the main factors that influence rainfall ISV over southern and central Vietnam. Linden, Fink, Pinto, et al. (2016) show daily rainfall associated with different phases of the MJO and equatorial waves. They also show that these waves enhance the frequency of intense daily rainfall during the wet phase, and interference between these different waves can lead to strong enhancement of wet or dry conditions. Yokoi et al. (2007), TT18 and TT19 also find that large-scale dynamics associated with rainfall variation resemble the MJO and tropical wave activity, especially for Central and South Vietnam. TT18 indicates a tropical Indian Ocean mode in the form of equatorial Rossby waves with 10–20 day variation in North and South Vietnam, and TT19 relates MJO activity to 20–60 day variations in South Vietnam.

Extratropical influence is commonly identified with pressure surges or cold surges from Siberian. Tuan (2019) finds that extratropical precursors to Vietnamese rainfall ISV often take the form of wave trains along with the North Atlantic–Asian North Pacific jet and that pressure surges from the Siberian high and Northeast China are associated with sub-monthly rainfall anomalies over North and Central Vietnam.

Individual wet events can also arise from an interplay between tropical and extratropical factors. Wu et al. (2012) show an example of a synoptic-scale tropical wave formed over the South China Sea combined with a surface high extending from western Mongolia to the East China Sea with a presence of strong MJO over the Indian Ocean leading to heavy rainfall. Further examples of combined effects involve tropical depressions associated with the summer MJO (Chen et al., 2012).

The main focus of this paper is on the asymmetries in large-scale dynamical precursors to opposite signs of anomalous rainfall: Wet and Dry episodes in selected sub-regions of Vietnam during summertime. Our work is intended to complement previous work where regional dependence has been expressed either as sub-regions or spatial patterns. Our choice of sub-regions is deliberately simple and we retain a relatively large scale compared to the linear nature of the country under consideration in order to ease the potential connection with dynamics at a larger scale compared to local phenomena. We will explicitly analyse composites for two sub-regions that include Vietnam: North and South, and we will also analyse an intermediate zone between them in order to address the scale of the anomalies considered. These regions will first be analysed separately and then their interdependencies will be investigated. Specifically, we address the following questions:

- Can we identify dynamical precursors/pathways of influence to anomalous rainfall over North and South Vietnam?
- How asymmetric are the precursors for Wet and Dry anomalies?
- How much do these precursors extend or overlap from one sub-region to another?
- How sensitive are our conclusions to choices of region, threshold, and composited quantity?

Data and methods are presented in Section 2. The regional development of the moisture budget terms associated with the composites is described in Section 3.

Section 4 then shows the large-scale dynamics associated with these composites. Discussion and conclusion are given in Section 5.

2 | DATA AND METHODS

2.1 | Data

We use 38 years (1979–2016) of ERA-Interim global reanalysis (Dee et al., 2011). Four-times daily data of atmospheric variables including zonal wind—u, meridional wind—v, specific humidity—q, and geopotential height—gph are used from a dataset that has been interpolated to $T42$ horizontal resolution on a 128×64 grid and set on sigma levels relative to mean sea level pressure for use in complementary studies with a dynamical model. Daily gridded 1×1 degree data of precipitation is used from ERA-Interim reanalysis (thereafter PPT) using the Frequent Rainfall Observations on GridS (FROGS) dataset (Roca et al., 2019).

We also use the following additional sources of precipitation data: APHRO and VnGP, to examine the sensitivity to the definition of our index. The APHRODITE-MA_V1101EX-R1 is downloaded from http://aphrodite.st.hirosaki-u.ac.jp (Yatagai et al., 2012) and the VnGP is high-resolution gridded data published in Nguyen-Xuan et al. (2016). In general, the spatial coverage of these datasets differs from the reanalysis product, as it is based on station data, which is unevenly distributed over the regions we consider. Details of these datasets are given in Table 1. We will examine the sensitivity of large-scale precursors to this difference.

The data are processed retaining the entire ISV signal. The only filter applied is to remove synoptic timescales. The four-times daily VIMC is calculated using u, v, and q at all levels, and then averaged to daily values for comparison with the PPT from ERAi-FROGs. All the data including three different rainfall datasets and VIMC are smoothed with a 10-day running mean. The annual cycle is calculated from daily mean values throughout the whole period of the dataset, also subject to a 10-day running mean filter to remove sampling variations. This smoothed annual cycle is subtracted from the data. Finally, the linear trend at each grid point time series is removed by linear regression to obtain intraseasonal and interannual variations. The gph at 250 mb and wind (u, v), velocity potential (VP), stream function (SF), and gph at 850 mb are also subjected to the same procedure to investigate the large-scale circulation.

In addition, El Niño Southern Oscillation (ENSO) is known to affect rainfall in Vietnam (Nguyen et al., 2013). Since our focus is on intraseasonal variability, dominant interannual ENSO-related signals are removed using the bi-monthly Multivariate ENSO Index—MEI time series provided by the National Oceanic and Atmospheric Administration at https://psl.noaa.gov/enso/mei/.

2.2 | Methods

Signals associated with anomalous rainfall are constructed using composites. This approach allows us to assess asymmetries in the moisture budget and large-scale dynamics associated separately with wet or dry conditions. It requires a regional index and a threshold that defines positive or negative episodes over the region.

The regional index is generated from the VIMC anomaly as outlined above. Each regional index is averaged over the domains. To analyse regional dependency (Nguyen et al., 2013; Tuan, 2019), and to analyse the encroachment of one region onto another we divided Vietnam into three regions included in the three boxes shown in Figure 1: North Vietnam—NVN; Central Vietnam and Central Highlands—CVN and South Vietnam—SVN. Note that these regions are relatively large compared to some previous studies and thus may display temporal characteristics that differ from those of station data. We concentrate on NVN and SVN in our composite analysis. A central intermediate region is also

TABLE 1 Data information.

DATA	Database	Spatial coverage	Period	Resolution
APHRODITE	Ground-based product	Land only		
	< 100 station over Vietnam	Monsoon Asia area	1979–2007	Grid 0.5°
		60° E–150° E × 15° S–55° N		
VnGP	Ground-based product	Land only		
	481 station over Vietnam	Vietnam mainland map	1980–2010	Grid 0.25°
ERAi—FROGs	Reanalysis product	Global coverage		
		Monsoon Asia area	1979–2016	Grid 1°

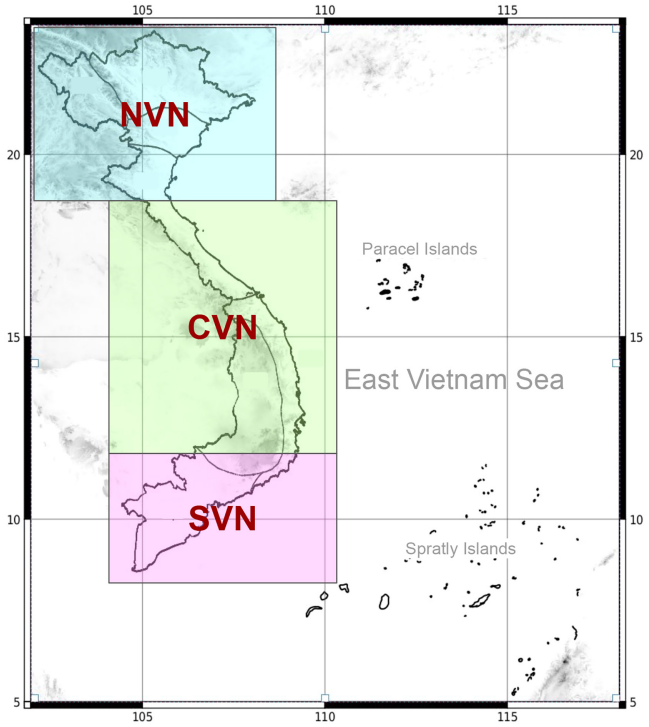

FIGURE 1 Vietnam map and selected regions: North Vietnam—NVN, Central Vietnam—CVN, South Vietnam—SVN. [Colour figure can be viewed at wileyonlinelibrary.com]

considered for which we also present statistics for the composite indices. Our CVN sits between NVN and SVN at a similar scale, but its region crosses the central mountain range and so integrates differing local rainfall signatures: rainfall peaks in the winter monsoon season in the eastern side and in the summer monsoon season in the southwestern part of the region, that is, the Central Highlands (Nguyen et al., 2013). CVN is included only to provide information on the extension of NVN and SVN indices into these central latitudes but does not necessarily provide detailed guidance for rainfall in a given location in central Vietnam. Sensitivity to the definition of these indices and to the rainfall dataset used will be discussed further below.

The threshold values were defined from the probability frequency distribution (PFD) of the daily VIMC index shown in Figure 2c, d. Following our regional PFD, the probability of days having intensity of rainfall anomaly above/below +3/−3 mm/day accounts for about 10% of the rainfall variability in all cases. A value of ±3 mm/day is also used in the hydrology sector to classify rainfall anomalies (Haensel et al., 2015). It can be used as a threshold value in this study to present opposing rainfall anomalies. We will discuss the sensitivity of our results to this choice below.

The composites are constructed from filtered daily anomalies of the VIMC index that exceed +3 and −3 mm/day, respectively. First, we concentrate on characteristics exclusive to each region by gathering composites for a given domain only, but not in the other two. This means that 'overlapping' dates having more than one regional index exceeding the threshold value are excluded from the composites. Further composites are then constructed that include the overlapping days to reveal the level of dependency between regions or the degree of extension of a rainfall signal outside the defined region. All dates that have regional VIMC anomalies greater than 3 mm/day are defined as Wet, and those less than −3 mm/day are defined as Dry. We will refer to these as Wet and Dry days but it should be remembered that we are using filtered anomaly indices, not actual daily rainfall.

Details of the number of days associated with all possible combinations for the three regions for Wet and Dry conditions are shown in Table 2. This table forms a symmetric matrix so the redundant upper right triangle is left blank, and impossible Wet–Dry combinations are marked 'none'. Total numbers of days are recorded, and in parentheses, we show the number of days when multi-region Wet or Dry conditions are excluded. The number in parentheses can only be non-zero on the leading diagonal and in the lower left quadrant. Specifically, there are 302, 277, and 172 exclusive Wet days for NVN, CVN, and SVN respectively, and 282, 267, and 277 exclusive Dry days.

Composite mean fields for diagnostics related to precipitation and circulation are calculated from all of these indices, and the results will be examined for asymmetry between Wet and Dry composites. To provide an objective measure of the degree of global pattern asymmetry, an asymmetry index is defined as $I_a = N_a/(N_s + N_a)$, where N_s is the number of grid points where Wet and Dry composites have the opposite sign and N_a where they have the same sign, for grid points where signals for both Wet and Dry composites are significant at the 95% level.

3 | REGIONAL DEVELOPMENT

3.1 | Regional climatology

Monthly averaged rainfall and monthly variance of daily anomalies of PPT and VIMC over NVN and SVN domains are shown in Figure 2c, d. The monthly variance of VIMC and PPT are similar and follow the seasonal cycle of rainfall, especially in NVN. Most of the rainfall occurs over both regions during the summertime (May–October). Monthly rainfall peaks in August in NVN (Figure 2a) and September–October in SVN (Figure 2b). The VIMC and PPT anomalies in NVN show maximum variance in line with maximum rainfall.

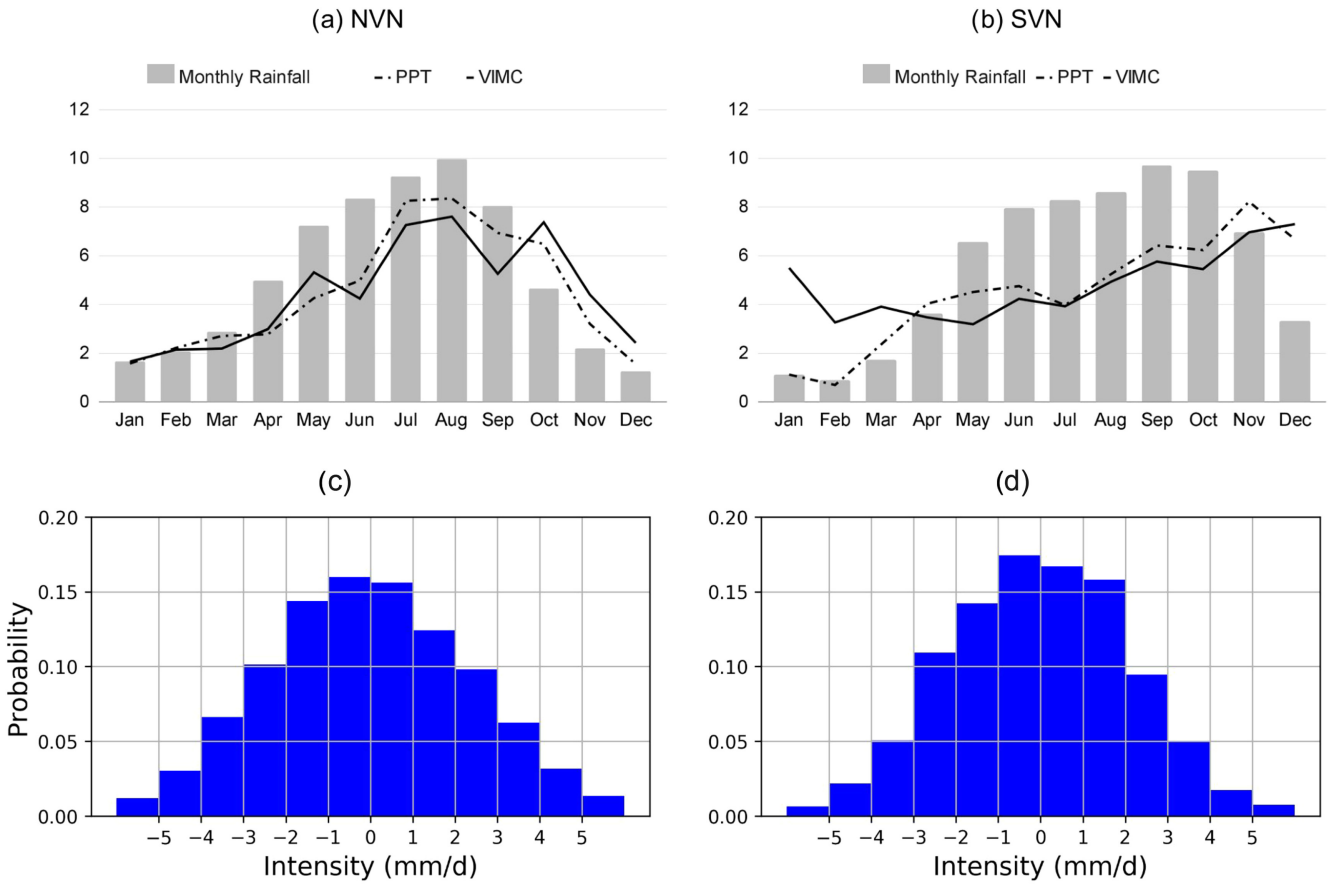

FIGURE 2 Monthly average of rainfall (grey bars) (mm/day) and monthly variance of daily time-series regional VIMC anomaly (solid line) and PPT (ERAi/FROGs) anomaly (dashed line) (mm^2/day^2) over (a) NVN, (b) SVN. Probability frequency distribution (PFD) of VIMC index over (c) NVN, (d) SVN. [Colour figure can be viewed at wileyonlinelibrary.com]

TABLE 2 The number of days that happened over regions N (North), C (Central), and S (South) of Vietnam with/without overlapping days shown out/in parentheses. Wet/Dry means exceeded +3 mm/day and −3 mm/day of VIMC.

	N wet	C wet	S wet	N dry	C dry	S dry
N wet	624 (302)					
C wet	322	745 (277)				
S wet	53	199	371 (172)			
N dry	None	0 (0)	34 (31)	493 (282)		
C dry	2 (0)	None	3 (0)	211	619 (267)	
S dry	93 (87)	4 (0)	None	29	170	447 (227)

The annual cycles of rainfall over the three regions show differences from previous regional rainfall studies due to the definitions chosen for the regions and the data used. Note that the seasonal cycle for CVN (not shown) is different from what it would be if data were restricted to the national territory. Our region includes an area to the west that is directly influenced by the summer monsoon in addition to the orographic influence of the Truong Son mountains that better characterises the Vietnamese coastal rainfall signal which peaks in September (TT19). For this reason, we do not present composites for this region but we retain it for information pertaining to the extension of the rainfall signal in the other two regions. For SVN, our selection covers flat terrain and a part of the sea, which is subject to a strong seasonal signal from the summer monsoon (Nguyen et al., 2013). The high rainfall intensity has a relatively low variance during the rainy season compared to the two other regions.

Temporal variations in VIMC are well correlated with the reanalysis rainfall product, and thus present a reasonable proxy to investigate directly the link between the hydrological cycle and the associated large scale circulation

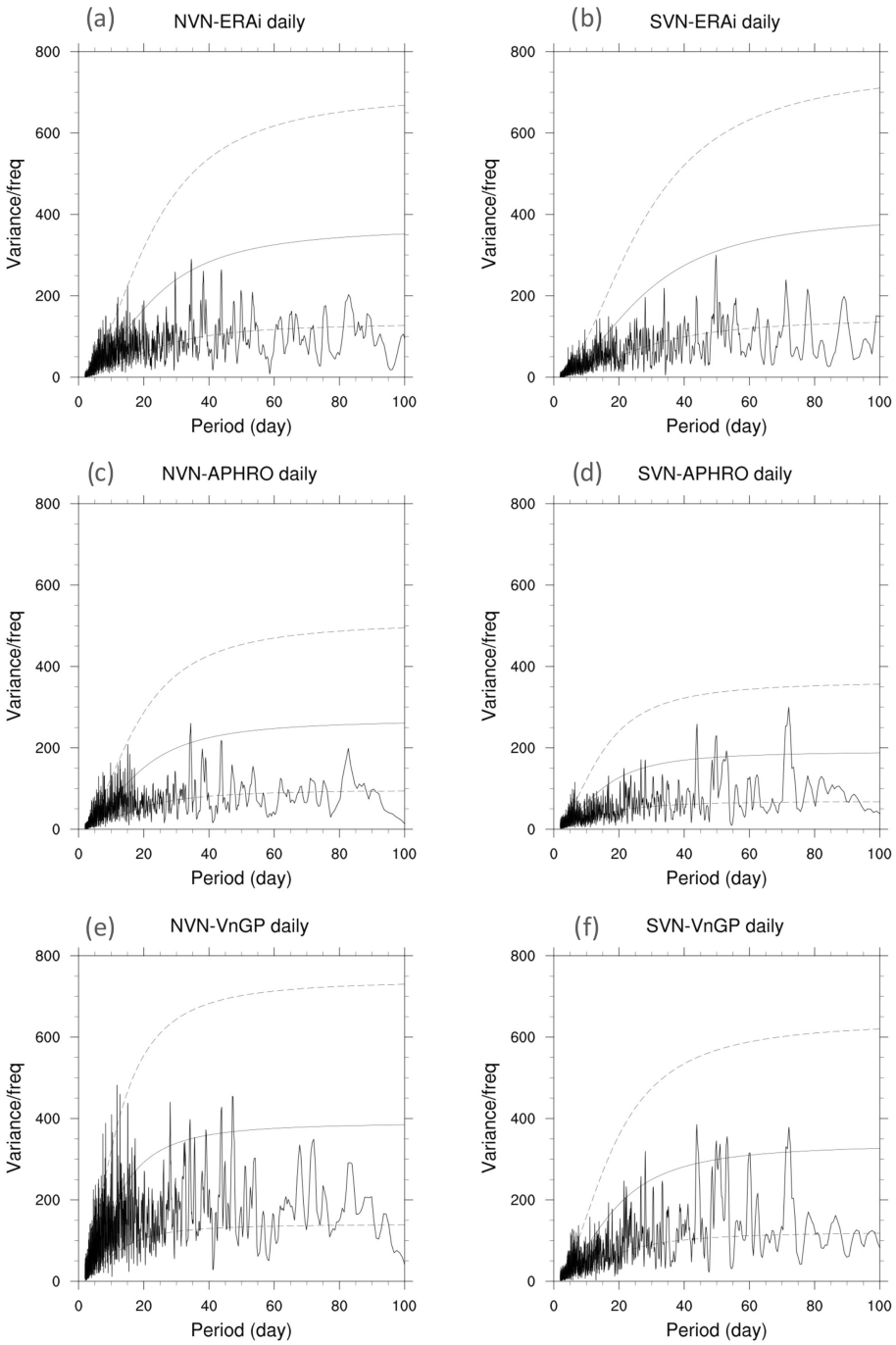

FIGURE 3 Variance spectra (black line) of the regional rainfall derived from ERAi (a), (b), APHRO (c), (d) and VnGP (e), (f) for NVN and SVN, respectively. The black curve is Markov red noise spectrum and the dash lines are 5% and 95% confidence interval bounds.

(Sohn et al., 2004). Chansaengkrachang et al. (2018) also show that VIMC shows a high positive correlation with the daily rainfall over Thailand.

Contributions to rainfall variability from different time scales are presented as variance spectra in Figure 3 for North and South Vietnam using the three different datasets. The spectral analysis of daily rainfall is performed without any filtering. It has some structure in the intraseasonal range and some differences between NVN and SVN, but most of the peaks like within the the 5%–95% confidence interval bounds. The spectrum of regional daily rainfall of VnGP shows peaks in the range of 10–45 days for NVN; 5–15 days and 20–75 days for SVN. Of the three datasets, VnGP shows the greatest variance in each sub-region but the positions of its spectral peaks are similar to those of APHRO, especially in SVN. The different amplitudes can be attributed to different interpolation methods as discussed in Nguyen-Xuan et al. (2016). Sub-monthly rainfall variability shows evidence of the peak identified by TT18 for NVN, and the longer range for SVN is likely to be linked to the influence of the MJO identified by Linden, Fink, Pinto, et al. (2016) and TT19. However,

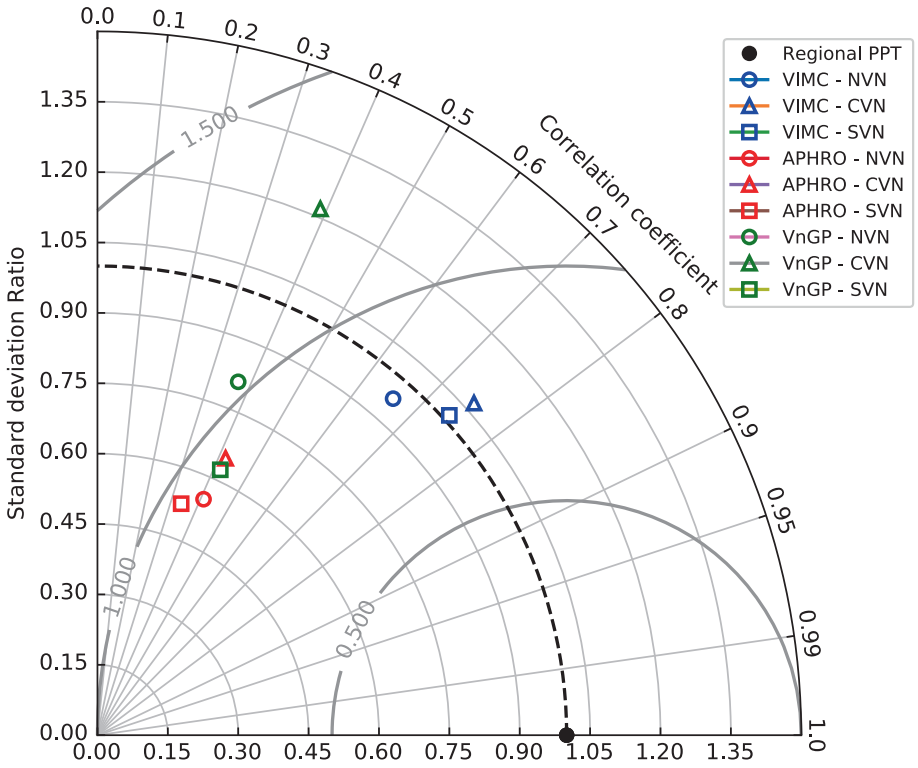

FIGURE 4 Comparison between regional daily-time series from May to October obtained from APHRO, VnGP, VIMC, and PPT (ERAi/FROGs). [Colour figure can be viewed at wileyonlinelibrary.com]

none of the datasets stray far from the red noise autoregressive curve and non-periodic behaviour may form an important component of regional variations. For this reason, we have chosen to limit the amount of filtering applied as described above. Our methodological choice is to include non-cyclic components of the variability, which are more likely to contribute to asymmetry in the composites.

The relationships between different datasets are summarised in Figure 4 in the form of a Taylor diagram for the daily-time series from May to October, averaged over our three regions for the APHRO, VnGP, VIMC, and PPT. The PPT from the reanalysis product ERAi/FROGs over each box is used as a reference: a black point on the lower axis. The root mean square difference from this reference is the linear distance to this black point (grey circles), the correlation coefficient is the angular distance, and the relative magnitude of the standard deviation is the radial distance from the dashed circle.

We see that the standard deviation of PPT is very similar over our three chosen regions, with 2.43 mm/day for NVN, 2.42 mm/day for CVN, and 2.22 mm/day for SVN.

The daily VIMC indices have a high positive correlation to PPT, with coefficients of 0.66 for NVN; 0.76 for CVN, and 0.72 for SVN. They are also very close to PPT in standard deviation for all three domains. The VnGP and APHRO indices both show a positive correlation with PPT of about 0.4 (and APHRO and VnGP indices are very highly correlated with one another: 0.93 for NVN, 0.78 for CVN, and 0.85 for SVN).

The APHRO indices show uniform variance, but it is weaker than for PPT with a ratio of 0.5–0.6. On the other hand, the VnGP CVN indices show a spread of variance: stronger than PPT for CVN and weaker for NVN and SVN.

These differences between data can mostly be attributed to the extent of the coverage. It can be seen that the ISV over CVN box is particularly sensitive to the dataset in use, undoubtedly for the reasons already discussed: VnGP covers Vietnam mainland only, thus representing the coastal region—east of the Truong Son mountains.

Since our focus is on large-scale precursors, we will proceed with VIMC as a proxy for the diagnosis of rainfall variability over NVN and SVN only, at the regional scale on intraseasonal timescales in the summertime. We will, however, examine the sensitivity to the choice of rainfall dataset for large-scale precursors to Wet and Dry conditions in section 4 below.

3.2 | Precipitation composites

The 2 week lagged composites of VIMC and PPT anomalies associated with Wet and Dry conditions at the regional scale are shown in Figures 5 and 6. In these and in the following figures lags of 15, 9, and 3 days have been chosen to represent the smooth time development over the 2 weeks prior to the simultaneous composite at day-0, to provide information on progressively

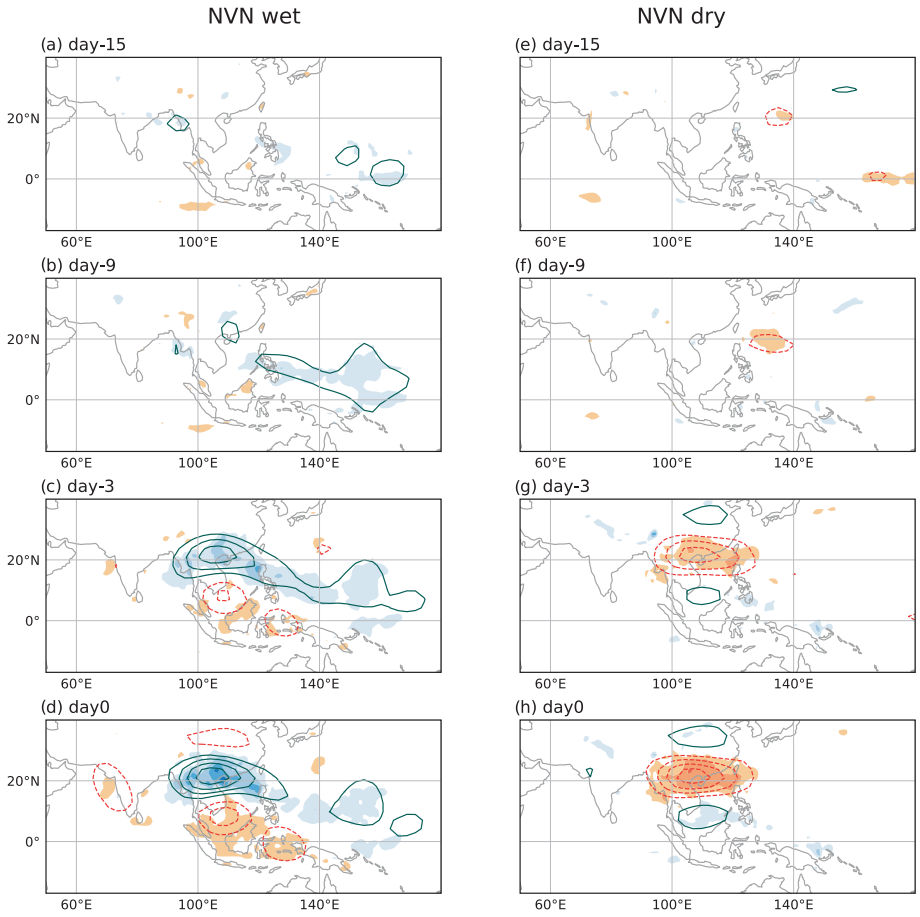

FIGURE 5 Composites of PPT anomaly (shaded colour) and VIMC anomaly (contour) associated with Wet (a)–(d) and Dry (e)–(h) composites in NVN. Blue is positive. Red is negative. Both the contour and colour interval are 1 mm/day. Plotted signals are statistically significant at 95% for each composite compared to the observation in a two-sided *t*-test. [Colour figure can be viewed at wileyonlinelibrary.com]

shifting anomalies with more time resolution towards the end.

Figure 5 shows spatial patterns for NVN. Positive anomalies of VIMC and PPT over the western Pacific can be seen from day-15 to day-0 (Figure 5a–d) prior to Wet composite days. VIMC anomalies develop to the northwest to cover NVN at day-9, accompanied by PPT anomalies. A wet-dry dipole over North–South Vietnam is established by day-3 for NVN Wet conditions. Dry conditions are more weakly foreshadowed in the lagged composites (Figure 5e–h), with negative VIMC and precipitation anomalies first occurring over the Western Pacific at 20° N and over NVN at day-3. The day-0 regional dipole over North–South Vietnam for Dry conditions is quite symmetrical between Wet composites, but only the Wet composite extends into the West Pacific.

Figure 6 shows lagged composites for SVN. Both Wet and Dry composites have significant VIMC and PPT anomalies from day-15, especially for Dry conditions. Wet conditions in SVN are associated with weak positive anomalies of VIMC and PPT over the Maritime Continent from day-15 which intensify to cover a large region, from the equatorial Western Pacific to the Indian Ocean (Figure 6a–d). A weaker negative anomaly from the northern Philippines (Figure 6e) moves gradually westwards to cover northern Vietnam. Dry composites in SVN on day-15 show significant positive VIMC and PPT anomalies extending from the north of Vietnam to the western Pacific. This broad feature then becomes progressively more concentrated over the north of Vietnam (Figure 6e–h). The negative anomalies over the Maritime Continent (Figure 6e) strengthen and extend at the same time to cover a similar region to the positive anomalies in the Wet composites. VIMC and PPT anomalies for Wet and Dry composites in SVN show dipole patterns over North–South of Vietnam at day-0 (Figure 6d, h). The anomaly centres are co-located with anomalies of opposite signs for NVN.

These rainfall anomaly patterns predominantly show a wet-dry dipole over Vietnam. This pattern emerges clearly in the full intraseasonal signal, and is in accord with the findings of Tuan (2019) and TT19 for 7–25-day and 20–60-day filtered rainfall data respectively. The principal asymmetry that we find is in the precursors, which are stronger and more extended into the Western Pacific for NVN Wet and SVN Dry.

4 | LARGE-SCALE CIRCULATION

In this section, the large-scale circulation associated with Wet and Dry composites is examined. Precursors will be

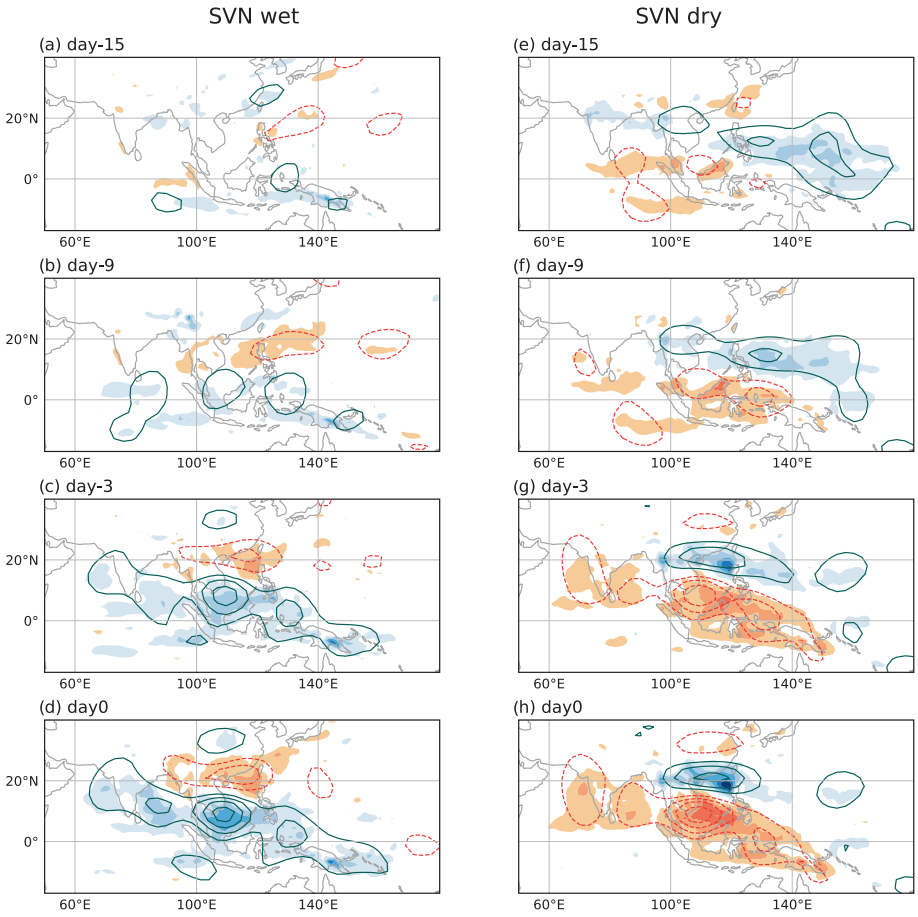

FIGURE 6 Same as Figure 5, but for SVN. [Colour figure can be viewed at wileyonlinelibrary.com]

analysed with attention to the degree of symmetry between Wet and Dry episodes and between regions. Diagnostics have been chosen to highlight both tropical and extratropical factors.

4.1 | Tropical flow

To look at tropical influence, we examine the low-level divergent and rotational flow. The following set of figures shows the velocity potential, SF, and wind vectors in the lower troposphere at 850 mb, relevant to anomalous moisture transport and its convergence.

Figure 7a–d shows the low-level flow at 850 mb associated with NVN Wet composites. There is a persistent low-level convergence anomaly from day-15 over the Western Pacific (Figure 7a) that is co-located with the positive VIMC anomaly (Figure 5a). It can be seen as a tropical precursor to Wet conditions in NVN. It intensifies over NVN from about day-9. At the same time, the westerlies intensify over Southeast Asia with both divergent and rotational components as a negative SF anomaly grows over the southern coast of China. This pattern propagates westwards and intensifies leading to a second centre of VP co-located with positive VIMC over NVN at day-0 (Figure 7d) and the peak in westerlies separates North and South Vietnam at the axis of the dipole in VIMC (Figure 5d). The low-level pattern for Dry composites over NVN has weaker precursors in the divergent flow than the Wet case (Figure 7e–h). There is a persistent low-level cyclonic flow off the coast of Japan and on day-9 large-scale low-level divergence develops to the west of this cyclonic flow. This intensifies rapidly over the following week to form a strong divergent centre over NVN co-located with negative VIMC (Figure 5h) and anticyclonic low-level flow. For both Wet and Dry cases, the low-level precursors at regional scale are to the east and appear to have their origins in the tropics (Wet composites) and the extratropics (Dry composites) associated with developments in divergent and rotational flows.

Low-level flow at 850 mb for SVN composites is shown in Figure 8. Here we see a positive anomaly in VP over the eastern Indian Ocean with a slow eastward displacement. For Wet conditions over SVN, there is also a weak large-scale divergent anomaly over the Pacific day-9 (Figure 8b) and easterly winds develop across the Philippines into southern Vietnam, associated with a dipole in SF. This easterly flow is a potential source of moisture transport and VIMC grows over SVN from

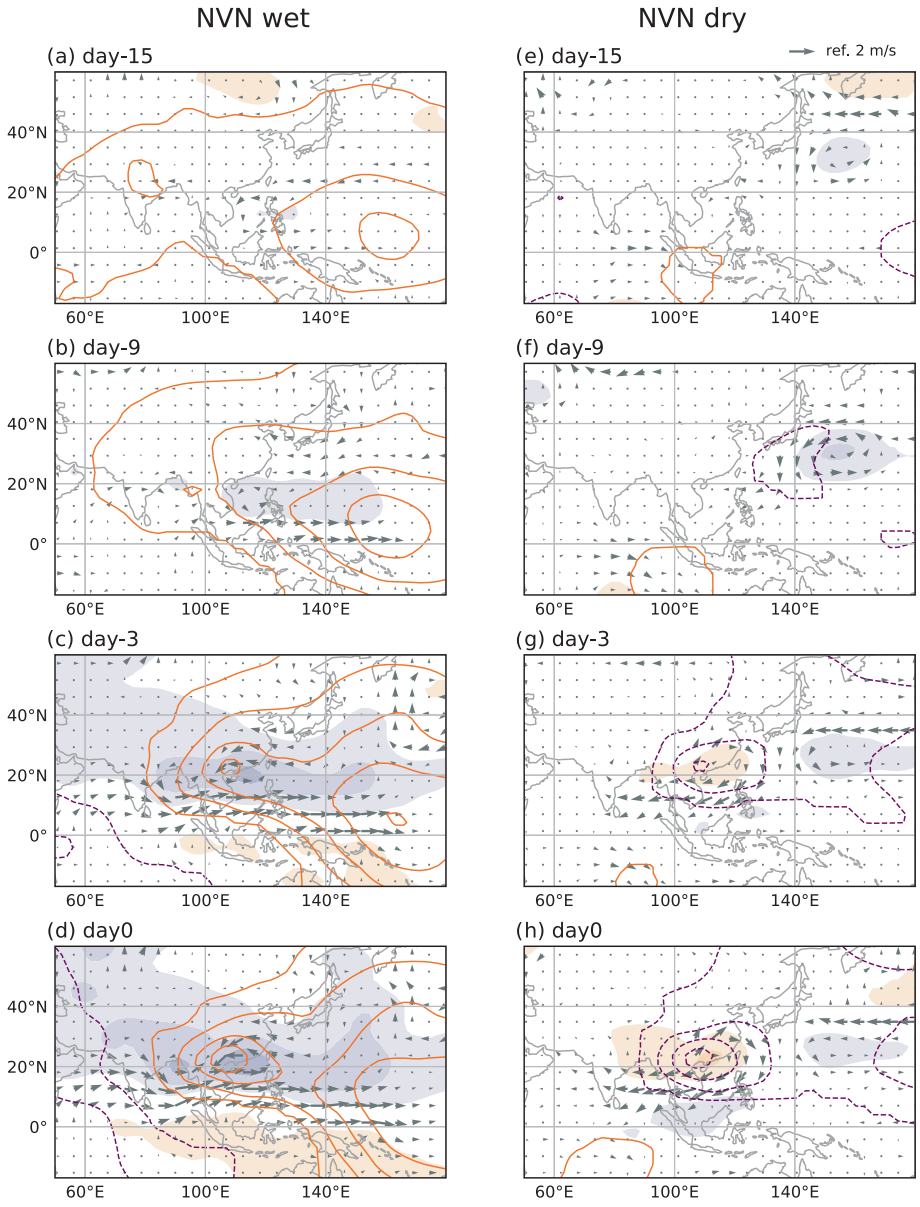

FIGURE 7 Composites of stream function (shaded colour), velocity potential (contour), and horizontal wind (vector) anomalies at 850 mb anomalies associated with Wet (a)–(d) and Dry (e)–(h) days over NVN. The purple colour (lines) is negative. The orange colour (lines) is positive. The contour interval is 2e5 m^2/s; and the colour interval is 6e5 m^2/s. The vector reference 2 m/s is in the top right corner. Plotted signals are statistically significant at 95% for each composite compared to the observation in a two-sided *t*-test. [Colour figure can be viewed at wileyonlinelibrary.com]

day-9 as it strengthens and the positive centre of VP intensifies and moves over the Maritime Continent. For Dry conditions (Figure 8e–h) there is large-scale convergence over the Western Pacific, followed by slow displacement from the equatorial Indian Ocean to the Maritime Continent. There is a low-level westerly jet associated with cyclonic flow and negative streamfunction over the Western Pacific at 20° N.

In summary, the precursors for NVN and SVN at regional scale are quite different. In all cases, maxima of VP are associated with VIMC centres, and there is also a strong rotational component to the anomalous circulation. For NVN the precursors are mainly to the east at regional scale and are quite asymmetric, with a tropical convergence for Wet cases and extratropical cyclonic flow for Dry cases. For SVN the tropical divergent flow displaces slowly eastwards in both cases, reminiscent of the development of the Summer MJO through phases 2–3 (Wet) or 6–7 (Dry) (Linden, Fink, Pinto, et al., 2016; Madden & Julian, 1972). The anomalies are quite symmetrical at regional scale except for the strong convergence over the Pacific for SVN Dry.

It is worth drawing attention to some similarities between the divergent flow for NVN Wet and SVN Dry composites. They share a convergence area over the Western Pacific, although for SVN-Dry the large-scale convergence area moves to the east and there is a weaker signal in VIMC over NVN while for NVN-Wet, the convergence area strengthens and develops westwards. The negative anomaly of VIMC over NVN in NVN Dry composites is associated with the local anticyclonic development with descending motion, but there is weaker vertical motion for SVN-Wet.

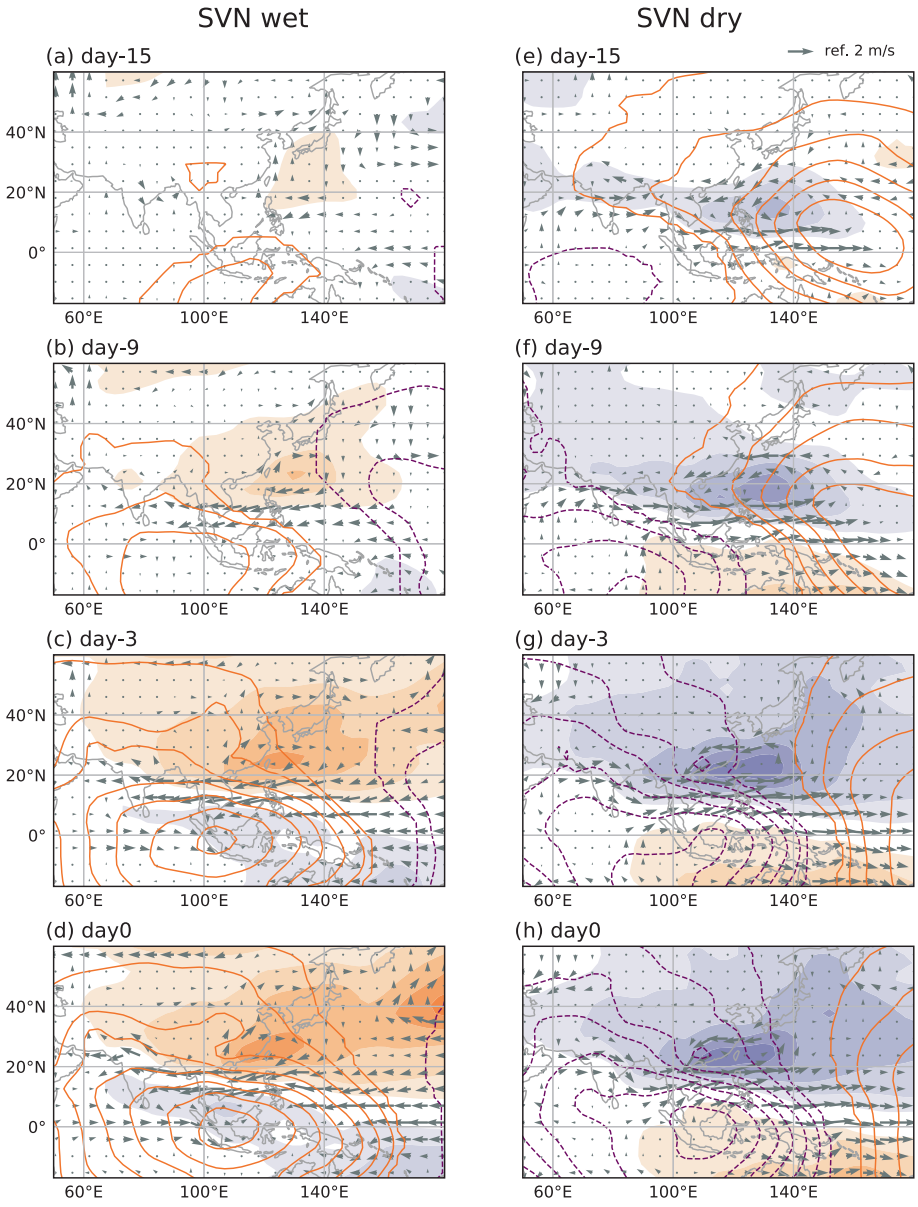

FIGURE 8 Same as Figure 7, but for SVN. [Colour figure can be viewed at wileyonlinelibrary.com]

4.2 | Extratropical flow

For the analysis of extratropical teleconnections, we examine the geopotential height in the upper troposphere at 250 mb and lower troposphere at 850 mb to diagnose geostrophic flow anomalies and their propagation over the preceding 2 weeks.

The Northern Hemisphere extratropical flow for Wet and Dry composites in NVN are shown in Figure 9 through 2 weeks of lagged composites of geopotential height anomalies at 250 mb and 850 mb. For Wet composites on day-15 (Figure 9a) a positive anomaly is situated over Europe and a negative anomaly over Kazakhstan. The high shows slight eastward displacement until day-9 and then dissipates, giving way to a low over Russia that subsequently grows on day-3 and spreads southwards quickly. At the same time, there is a persistent stationary high over Eastern Siberia that extends over Japan. All these features are equivalent barotropic with anomalies aligned between lower and upper levels. At lower latitudes a barotropic high starts to displace eastwards, south of the Asian jet until day-0 (Figure 9d) as a low develops over China that is tilted to the northwest with height.

Dry conditions in NVN are associated with a large-scale equivalent barotropic negative anomaly over Eastern Europe that strengthens and extends southwards into the jet region from day-15 to day-9 (Figure 9e, f). During this period there is an equally strong negative anomaly further east over northern China/Mongolia, and there is a persistent upper-level high between the two negative centres. This low–high–low structure sits on the Asian jet axis and shows very slight phase propagation to the east.

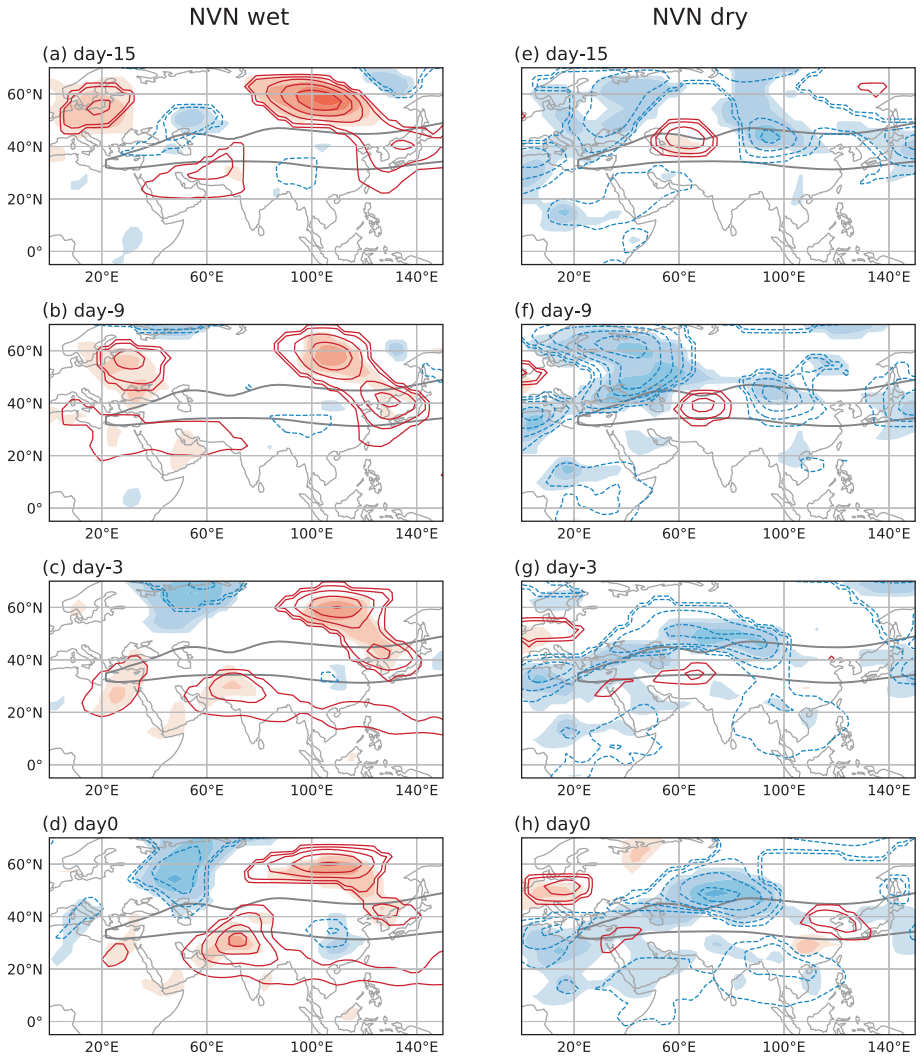

FIGURE 9 Composites of geopotential height anomalies at 850 mb (shaded colour) and at 250 mb (contour); jet stream (black line) indicating summer climatology $u_{250mb} > 20$ m/s at 250 mb associated with Wet (a)–(d) and Dry (e)–(h) composite days over NVN. The red colour (lines) is positive. The blue colour (lines) is negative. The colour (contour) interval is 1 (5) m. Plotted signals are statistically significant at 95% for each composite compared to the observation in a two-sided *t*-test. [Colour figure can be viewed at wileyonlinelibrary.com]

Sub-region	Diagnosis	Day-15	Day-12	Day-9	Day-6	Day-3	Day-0
NVN	gph 250 mb	0.15	0.14	0.22	0.35	0.29	0.39
	gph 850 mb	0.06	0.05)	0.14	0.30	0.23	0.34
SVN	gph 250 mb	0.43	0.38	0.27	0.21	0.26	0.28
	gph 850 mb	0.39	0.34	0.21	0.13	0.19	0.22

TABLE 3 Asymmetrical index I_a between Wet and Dry composites over the extratropical area defined as 30–70 N and 0–150 E.

From day-3 to day-0 (Figure 9g, h) the two low centres merge and spread towards South-East Asia while the positive anomaly dissipates and a new positive anomaly centre is established over China–Korea–Southern Japan. These developing features that appear along the jet axis are baroclinic in nature and the positive anomalies have weak surface expression.

Comparing Wet and Dry precursor developments for NVN we see considerable asymmetry at high latitudes. The asymmetrical index I_a defined in Section 2 is displayed in Table 3, with values increasing from 0.06 to 0.34 for geopotential height anomaly at 850 mb and from 0.15 to 0.39 for those at 250 mb. The asymmetry is strongest for long lead times at high latitudes as there is no counterpart in the Dry composite to the persistent high over Siberia seen for the Wet composite. Although both series show alternating signs along the jet, they are not in phase opposition and they have different characteristic scales. The NVN-Wet precursors spread on both sides of the jet, while NVN-Dry precursors are more confined to the jet region. Precursor signals are thus also asymmetric at lower latitudes.

Note that on day-0 there is a low-level geopotential height anomaly over China, negative for Wet and positive for Dry. These features are baroclinic (tilted with height) and ageostrophic, as they are slightly displaced relative to

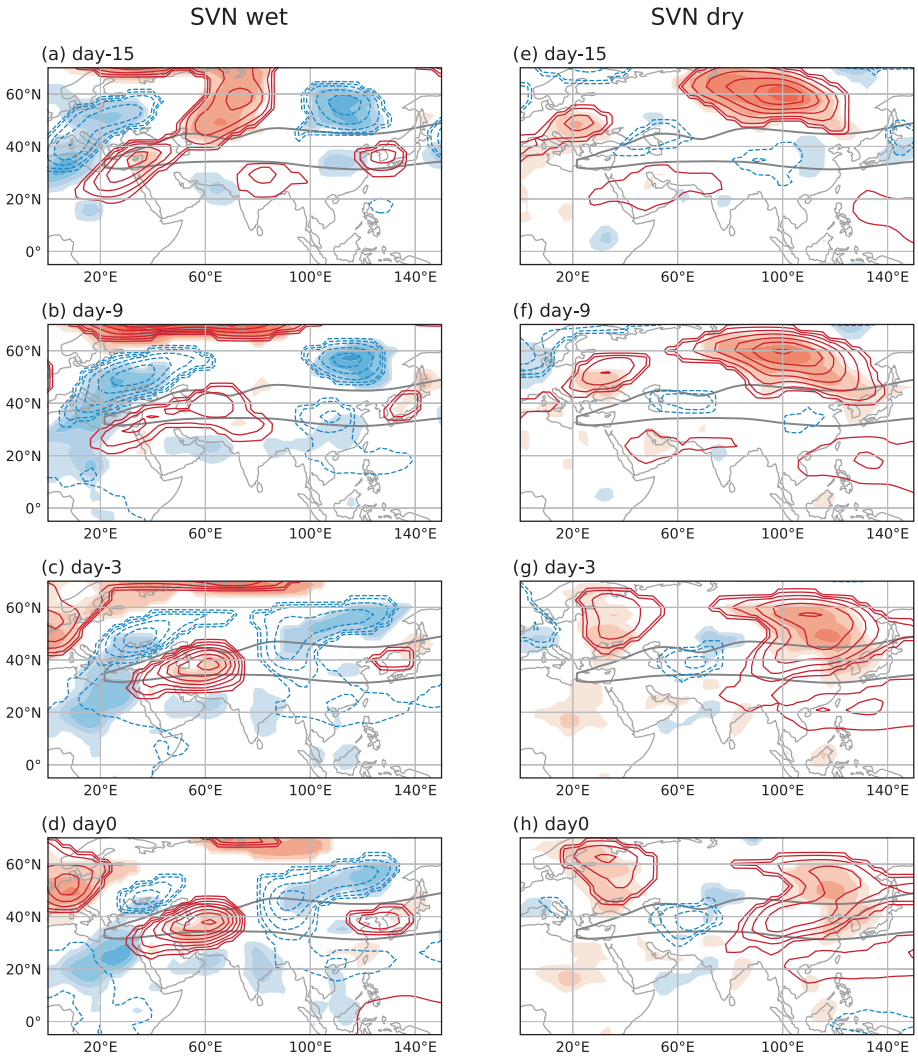

FIGURE 10 Same as Figure 9, but for SVN. [Colour figure can be viewed at wileyonlinelibrary.com]

the cenres of rotational and divergent flow, that in both cases are situated over the coast and into Northern Vietnam (Figure 7).

Figure 10 shows composites for SVN Wet and Dry anomalies. Both composites are associated with remarkably strong signals compared to NVN. Wet conditions are associated with an equivalent barotropic low over Siberia and a compact baroclinic upper-level high over Korea–Japan throughout the preceding 2 weeks. Further west, precursors take the form of an extended low and high, orientated SW–NE over eastern Europe/Asia. This structure tilts into the Asian jet from day-15 to day-9 (Figure 10a, b), after which a compact high intensifies in situ in the jet entrance. It becomes more baroclinic as it intensifies southwards. Although there is no discernible phase propagation, the signal intensifies eastwards at the latitude of the jet, finally establishing the upper-level high over Korea. The co-location of anomaly centres with mean position of the jet core is reminiscent of the dry composite for NVN.

For SVN dry composites, precursors are dominated by a persistent barotropic high over Siberia which is present from day-15 (Figure 10e). It intensifies on day-9 and then spreads southwards over China from day-3 to day-0. There is also a high over eastern Europe and a baroclinic low over the jet which moves slightly to the east from day-15 to day-9 and then intensifies until day-0. This pair of anomalies and the persistent high over Siberia are opposite to those seen for SVN Wet composites, so in this respect, there are symmetric precursors between Wet and Dry conditions. In Table 3, the asymmetry index I_a has values decreasing from 0.39 to 0.22 for geopotential height anomaly at 850 mb and from 0.43 to 0.28 for those at 250 mb. The overall patterns of extratropical flow associated with SVN Wet/Dry anomalies show some similarity to the composites for NVN Dry/Wet, although there are some differences in detail. The high-latitude anomalies over Europe are stronger and more stationary for SVN. A strong feature of the regional flow for SVN composites is the reversal of the zonal wind in the South China Sea. Just to the north of this, there are upper-level geopotential height anomalies associated with anticyclonic flow for Wet and cyclonic flow for Dry conditions.

4.3 | Regional interdependency

The analyses presented up to this point have been based on composites that exclude days in which the threshold is exceeded in more than one region. This operation has been carried out separately for Wet and Dry composite days, so the prominent Wet–Dry opposition between NVN and SVN is retained. But there are many excluded days where, for example, wet conditions extend from the NVN as we have defined it, into our artificial CVN region to the south. In this section, we examine how the results are affected by including these composite days in the analysis.

Table 2 shows that the CVN zone often shares Wet or Dry composite days with NVN or SVN. Generally, about half the Wet days and about one-third of the Dry days in either NVN or SVN extend into CVN. On the other hand, NVN and SVN are relatively independent from one another. They rarely share Wet conditions, but they are more commonly in opposition, consistent with some of the symmetries in composite patterns we have seen. The exclusion of the overlap with CVN makes very little difference to the frequency of NVN–SVN opposition.

How do the composite patterns change when shared composite days are permitted? After all, anomalies in a given region are of practical interest, regardless of how unique they may be. The extratropical flow associated with anomalous conditions shared by more than one region is shown here and compared with the isolated cases. The differences between these figures serve to illustrate how dependent these precursor diagnostics are on the definition of the regional index.

Figure 11 shows the large-scale precursors at day-0 when NVN and CVN are both wet (Figure 11a, c, e) or both dry (Figure 11b, d, f). The large-scale rainfall and VIMC anomalies (Figure 11a, b) are associated with a weaker tropical divergent flow as comparing between Figure 11c, d and Figure 7d, h. Both divergent and rotational flow show more symmetry between Wet and Dry conditions covering NVN and CVN. For the extratropical flow, the final state at day-0 shows a stronger signal. The pattern is largely in phase with the isolated NVN pattern with equivalent barotropic including a low over China that spreads from 60° N to 30° N and is more tilted with height. Dry composites show equivalent barotropic with strong anomalies aligned with height, essentially along the latitudes of the jet. Wet and Dry composite when NVN and CVN are now in the same conditions show more symmetrical than the isolated NVN.

A similar exercise can be carried out for common composite days between SVN and CVN and the resulting composites at day-0 are shown in Figure 12. The rainfall and VIMC anomaly patterns show a more emphatic signal along Vietnam's coast as in Figure 12a, b compared to

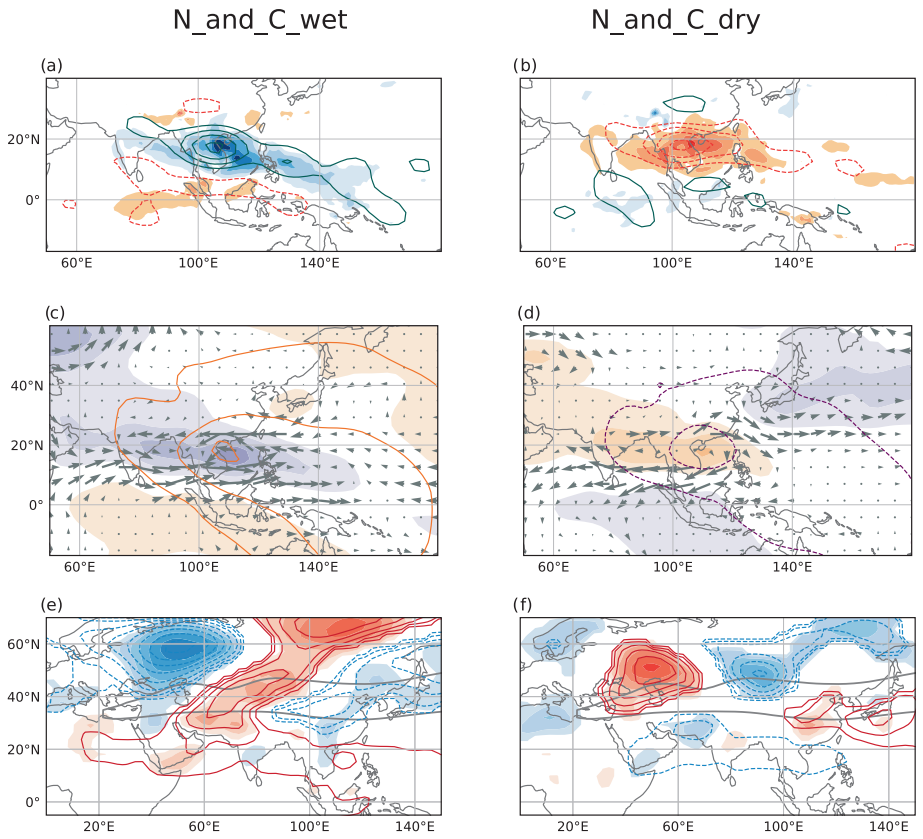

FIGURE 11 (a) and (b) same as Figure 5; (c) and (d) same as Figure 7; (e) and (f) same as Figure 9, but for the overlapping of North and Central (N_and_C) Wet (left) and Dry (right) composite, respectively at day-0. [Colour figure can be viewed at wileyonlinelibrary.com]

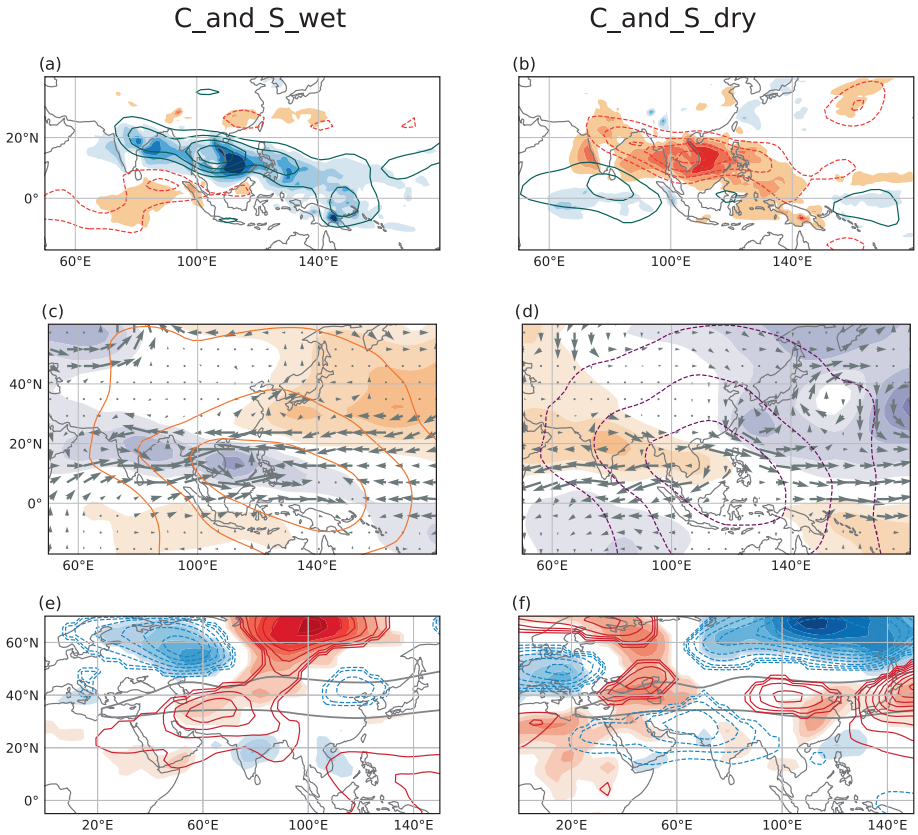

FIGURE 12 Same as Figure 11, but for the overlapping of Central and South (C_and_S) composites. [Colour figure can be viewed at wileyonlinelibrary.com]

Figure 6. The tropical flow associated with opposite patterns exhibits weaker signals in both divergent and rotational parts compared to isolated SVN (Figure 12c, d vs. Figure 8d, h). However, the extratropical flow in both Wet and Dry composite displays a great difference between isolated and extended SVN Figure 12e, f vs. Figure 10. Figure 12e, f shows stronger signal, equivalent barotropic at high latitude, and still quite symmetry in phases of anomaly. These patterns resemble the extratropical flow associated with the extended NVN composites than those of extended SVN.

In all cases, the tropical circulation shows less sensitivity than the extratropical one to the definition of the index for NVN and SVN, for both Wet and Dry composites. Anomalies that extend into the CVN zone are almost identical with a stronger signal in extratropical flow and a weaker tropical divergent flow in most cases and seem to be dominant by CVN's characters.

Finally, it is of interest to examine cases where NVN and SVN have opposite rainfall anomalies. Figure 13 shows large-scale composites from the 87 cases of NVN-Wet/SVN-Dry and the 31 cases with NVN-Dry/SVN-Wet. Recall that there is a close resemblance between composites for exclusive NVN-Wet and SVN-Dry. Figure 13a–d again shows a similar pattern but with much higher amplitude emphasized by greater contour and colour intervals, implying that although the NVN-Wet/SVN-dry pattern represents a relatively small number of days, they are among the strongest in terms of large-scale precursors. The NVN-Dry/SVN-Wet composite also shown in Figure 13e–h looks like a strongly amplified version of SVN-Wet, which was already somewhat stronger than NVN-Dry. Both cases apparently show the propagation of anomalies over Eurasia, most likely those of NVN cases. The extratropical flow of NVN-Wet/SVN-Dry composite at 40–60 N band shows a barotropic equivalent developing flowing the lag-composite, but not for NVN-Dry/SVN-Wet.

4.4 | Sensitivity to index definition

In this section we present a brief summary of results for alternative indices, APHRO and VnGP, to see how sensitive our results are to the type of rainfall data used. As presented in the data comparison, we note that the threshold for regional indices varies with the variance on the intraseasonal timescale, so in the following, the thresholds have been chosen so that these composites account for a similar fraction of the variance.

For NVN, based on PFDs as mentioned in Section 2, the threshold value for VnGP is 3 mm/day as it is for VIMC, but for APHRO it is 1.6 mm/day. Composites are assembled by applying the same process as for VIMC. The NVN Wet/Dry composites include 302/282 days for

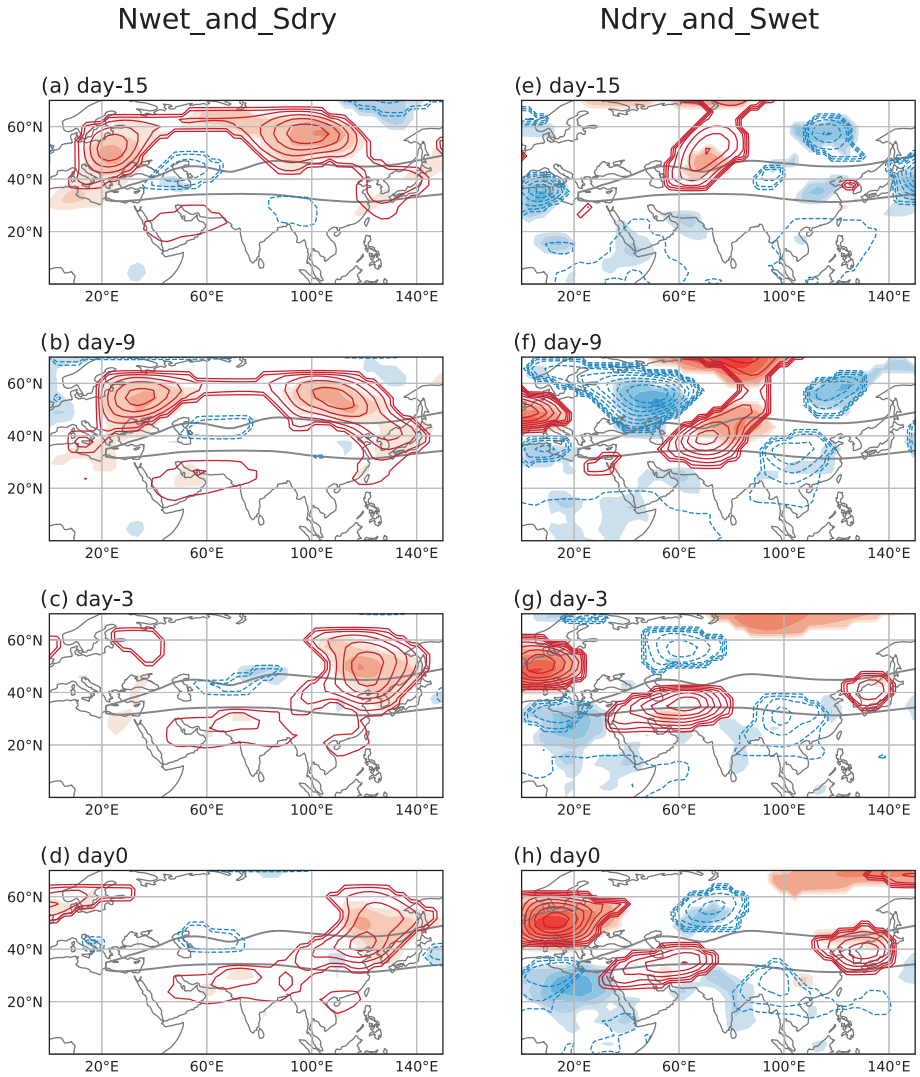

FIGURE 13 Same as Figure 9, but for the overlapping of Wet-NVN/Dry-SVN (Nwet_and_Sdry) (a)–(d) and Dry-NVN/Wet-SVN (Ndry_and_Swet) composites (e)–(h). The colour (contour) interval is 2 (8) m. [Colour figure can be viewed at wileyonlinelibrary.com]

VIMC, 372/222 days for APHRO, and 303/199 days for VnGP. For SVN, the threshold value for VnGP is 1.5 mm/day, and for APHRO it is 1.6 mm/day. The SVN Wet/Dry composites include 172/227 days for VIMC, 267/123 days for APHRO, and 315/192 days for VnGP.

Figure 14 shows composite large-scale geopotential height anomalies for 9-day lead times for NVN composites. These plots can be compared with the second row of Figure 9 for ERAi. For wet conditions over NVN, we see the 9-day precursors for these two datasets are in broad agreement. They share a north–south low–high dipole over western Asia and a double-high structure over northern Siberia extending over Japan. This latter feature is also present for the ERAi composite but further to the west the structures differ. For dry conditions, the very broad low over central and western Asia is recovered for all three indices, although it is weaker for ERAi. The high over Europe is also common to the three datasets, while there is some difference in the placement of smaller-scale positive anomalies. The broad agreement of phase for the three indices persists to day-0 (not shown).

Figure 15 shows the results for SVN (to be compared with the second row of Figure 10). In this case, for wet composites, there is quite a good agreement between APHRO and ERAi, but the VnGP composite is somewhat weaker and does not produce the same phase over northern and eastern Europe, or the high over eastern China–Japan. VnGP gives higher amplitude precursors for dry anomalies which are in phase at a large scale with those from APHRO, at least for eastern Asia. For dry anomalies, the ERAi composite differs, with the dominant large-scale high further north. Over western Asia and Europe, none of the indices show much consistency. As the lag progresses to day-0 the inconsistency between the three indices remains (not shown).

In general, the composites are fairly consistent for NVN, and as might be expected the APHRO and VnGP products are more similar to one another than they are to ERAi. For SVN we see a different story, with less

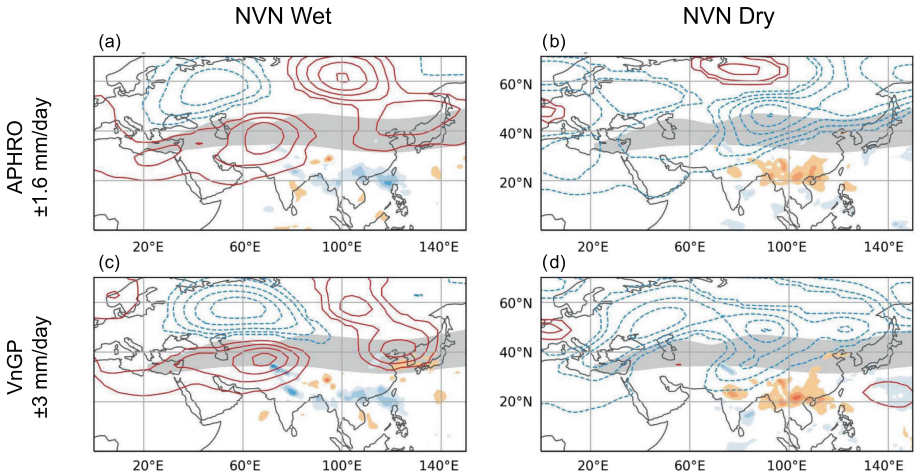

FIGURE 14 Composite of gph anomaly at 250 mb (contour lines) and precipitation anomaly (colour shaded) associated with the NVN Wet (left) and Dry (right) composites at day-9 that assembled from APHRO (a—372 days, b—222 days) and VnGP (c—303 days, d—199 days) indexes. The contour line interval is 8 m with red/blue being positive/negative. The colour interval is 1 mm/day with blue/orange being positive/negative. [Colour figure can be viewed at wileyonlinelibrary.com]

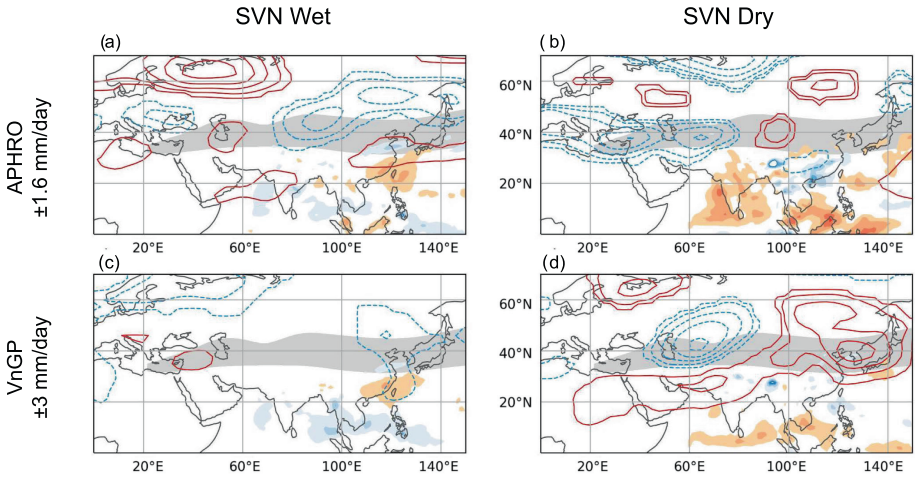

FIGURE 15 Composite of gph at 250 mb anomaly (contour lines) and precipitation anomaly (colour shaded) associated with the SVN Wet (left) and Dry (right) composites that assembled from APHRO (a—267 days, b—123 days) and VnGP (c—315 days, d—192 days) indexes. The contour line interval is 8 m with red/blue being positive/negative. The colour interval is 1 mm/day with blue/orange being positive/negative. [Colour figure can be viewed at wileyonlinelibrary.com]

consistency between any of the datasets. We conclude that precursor anomalies can be sensitive to the definition of index, especially in SVN.

5 | DISCUSSION

In this study, we have considered intraseasonal rainfall anomalies over three regional scale zones centred on Vietnam and explored remote dynamical influences. The investigation focuses on anomalous rainfall days in filtered daily data during the summertime with a lead time of 2 weeks. We have used the VIMC as a link between regional precipitation and large-scale dynamics, after first establishing that it is well correlated with intraseasonal rainfall variability on these time scales and can thus be reasonably used as a proxy.

The main focus of this work is to record the larger-scale dynamical environment associated with anomalies in regional hydrology. Vietnam is subject to diverse influences and we have seen that they combine in a variety of ways depending on the region. One of the difficulties in assigning causes to anomalies in a given region is the dependency between neighbouring and even distant regions. Another difficulty is the asymmetry often recorded between Wet and Dry composites. These two difficulties are the main theme of this paper, and for this reason, we have chosen to treat Wet and Dry anomalies separately, using composites rather than regressions, and avoiding restrictive time filtering that might hide non-periodic and asymmetric components of the variability. We have paid particular attention to the interdependency between regions by explicitly considering them in isolation and in combination.

When we break down the large-scale composites and examine them for Wet–Dry, north–south, and tropical–extratropical relationships, a complex picture emerges, as follows.

- Wet conditions in NVN are essentially influenced by the extratropics, but in a highly asymmetric way and also in a way that is very dependent on whether the anomalies in VIMC also spread south to the intermediate CVN zone. Isolated NVN anomalies are associated

with a barotropic Western high over Siberia and a baroclinic depression over China. For anomalies that also spread to CVN the precursors are quite different but still essentially north of the mean latitude of the Asian jet, with a low over Siberia developing into a three-pole large-scale low–high–low structure.
- Isolated Dry anomalies in NVN are highly asymmetrical compared to the Wet case. They are influenced by anomalies that line up along the latitude of the Asian jet, leading to an upper-level high over Korea and a low-level anticyclone over China. For anomalies that extend into the CVN zone, we recover a large-scale high–low–high pattern over Asia that is quite symmetrical with the corresponding Wet cases.

We conclude that for NVN there are two extratropical pathways of influence: large-scale barotropic quasi-stationary patterns at high latitudes in the Wet case and smaller-scale baroclinic perturbations along the jet in the Dry case. However, it must be stressed that for NVN the large-scale precursors are quite sensitive to the index considered and can show a great deal of asymmetry for Wet and Dry anomalies.

- Wet conditions in SVN are associated with a sequence of sign reversals along the mean position of the Asian jet, somewhat similar to Dry NVN, although the SVN Wet composites have larger amplitude than the NVN Dry ones, and precursors over western Asia are quite different. Furthermore, SVN is distinguished from NVN by the strong influence of a slowly moving buildup of low-level convergence over the Indian Ocean towards the Indonesian region, and a strong easterly flow anomaly over Southeast Asia reminiscent of the MJO (Linden, Fink, Pinto, et al., 2016). When SVN Wet is combined with NVN Dry the resulting composites are particularly intense but dominated by the SVN Wet pattern. Such a combination is perhaps selecting the strongest SVN Wet anomalies.
- Dry composites in SVN resemble Wet composites in NVN at high latitudes. This is where Table 2 reveals the greater overlap. Precursors are dominated by a high over western Siberia, but it now spreads further southwards, and an anticyclone appears over China. The combined composite is again more intense than either of the isolated composites. The equatorial influence for SVN Dry is not the opposite of the Wet case. This time the influence builds up in the east in the form of West Pacific convergence at considerably longer lead times before giving way to slowly eastward propagating low-level divergence over the region.

There are essentially three conduits of influence at lead times of one to 2 weeks:

1. A high latitude pathway where large-scale quasi-stationary equivalent barotropic patterns slowly build and then spread southwards to influence the region, particularly for NVN Wet and SVN Dry.
2. A pathway along the Asian jet, with smaller-scale baroclinic anomalies of alternating sign, showing eastward group propagation to influence NVN Dry and SVN Wet anomalies.
3. An equatorial pathway with slow eastward propagation of the asymmetric precursors in the divergent flow influencing SVN Wet and Dry anomalies.

The link between these extratropical developments and regional moisture flux convergence follows the development of low-level circulation anomalies with rotational centes near the south coast of China and centres of divergent flow over the region that are particularly distinct for NVN.

In a purely diagnostic study such as this one, care should be taken in attributing composite VIMC anomalies to circulation centres that develop prior to their emergence. For example, it is possible that the regional structures associated with SVN anomalies in VIMC are themselves a consequence of tropical propagating modes and not a direct cause of the VIMC anomaly. In this study, we have nevertheless identified some precursors that owe their existence to a range of phenomena associated with the pathways outlined above. These phenomena include Rossby wave propagation on the climatological extratropical flow, the development of baroclinic disturbances on the midlatitude jet, tropical waves, and the MJO. Extratropical pathways are likely to vary as the basic state changes throughout the season, and variations in the waveguide will impact both propagation and growth characteristics of the precursors. As already established in previous work, The southern region is directly influenced by tropical wave propagation. These considerations will be explored in a subsequent contribution using a global dynamical model. Further modelling work is needed to account for the causality of teleconnections documented in this study, in this highly diverse and sensitive region.

AUTHOR CONTRIBUTIONS

Hong-Hanh Le: Data curation; formal analysis; visualization; writing – original draft; writing – review and editing. **Nicholas M. J. Hall:** Conceptualization; methodology; writing – review and editing; supervision; writing – original draft. **Thanh Ngo-Duc:** Conceptualization; writing – review and editing; supervision.

ACKNOWLEDGEMENTS

Hong Hanh Le was funded by a PhD contract from the French Ministry of Education and Research. ERA-interim data are available at www.ecmwf.int. FROGs dataset are available at ftp://ftp.climserv.ipsl.polytechnique.fr/FROGs/. We would like to thank Pascal Roucou and Marine Herrmann for helpful discussions; and the two anonymous reviewers for their helpful comments, which greatly improved the quality of this work.

DATA AVAILABILITY STATEMENT

The data that support the findings of this study are available from the corresponding author upon reasonable request.

ORCID

Hong-Hanh Le https://orcid.org/0000-0003-0376-931X

REFERENCES

Chansaengkrachang, K., Luadsong, A. & Aschariyaphotha, N. (2018) Vertically integrated moisture flux convergence over southeast Asia and its relation to rainfall over Thailand. *Pertanika Journal of Science & Technology*, 26(1), 235–246.

Chen, T.-C., Yen, M.-C., Tsay, J.-D., Thanh, N.T.T. & Alpert, J. (2012) Synoptic development of the Hanoi heavy rainfall event of 30–31 October 2008: multiple-scale processes. *Monthly Weather Rev*, 140(4), 1219–1240. Available from: https://doi.org/10.1175/MWR-D-11-00111.1

Dee, D.P., Uppala, S.M., Simmons, A.J., Berrisford, P., Poli, P., Kobayashi, S. et al. (2011) The era-interim reanalysis: configuration and performance of the data assimilation system. *Quarterly Journal of the Royal Meteorological Soci*, 137(656), 553–597. Available from: https://doi.org/10.1002/qj.828

Haensel, S., Schucknecht, A. & Matschullat, J. (2015) The modified rainfall anomaly index (mRAI)—is this an alternative to the standardised precipitation index (spi) in evaluating future extreme precipitation characteristics? *Theoretical and Applied Climatology*, 1–18, 827–844. Available from: https://doi.org/10.1007/s00704-015-1389-y

Linden, R.V.D., Fink, A.H., Phan-Van, T. & Trinh-Tuan, L. (2016) Synoptic-dynamic analysis of early dry-season rainfall events in the Vietnamese central highlands. *Monthly Weather Review*, 144(4), 1509–1527. Available from: https://doi.org/10.1175/MWR-D-15-0265.1

Linden, R.V.D., Fink, A.H., Pinto, J.G., Phan-Van, T. & Kiladis, G.N. (2016) Modulation of daily rainfall in southern Vietnam by the madden–julian oscillation and convectively coupled equatorial waves. *Journal of Climate*, 29(16), 5801–5820. Available from: https://doi.org/10.1175/jcli-d-15-0911.1

Madden, R.A. & Julian, P.R. (1972) Description of global-scale circulation cells in the tropics with a 40–50 day period. *Journal of Atmospheric Sciences*, 29(6), 1109–1123. Available from: https://doi.org/10.1175/1520-0469(1972)029⟨1109:DOGSCC⟩2.0.CO;2

Nguyen, D.-Q., Renwick, J. & McGregor, J. (2013) Variations of surface temperature and rainfall in Vietnam from 1971 to 2010. *International Journal of Climatology*, 34(1), 249–264. Available from: https://doi.org/10.1002/joc.3684

Nguyen-Xuan, T., Ngo-Duc, T., Kamimera, H., Trinh-Tuan, L., Matsumoto, J., Inoue, T. et al. (2016) The Vietnam gridded precipitation (VnGP) dataset: construction and validation. *Scientific Online Letters on the Atmosphere*, 12, 291–296. Available from: https://doi.org/10.2151/sola.2016-057

Roca, R., Alexander, L.V., Potter, G., Bador, M., Jucá, R., Contractor, S. et al. (2019) Frogs: a daily 1 × 1 gridded precipitation database of rain gauge, satellite and reanalysis products. *Earth System Science Data*, 11(3), 1017–1035. Available from: https://doi.org/10.5194/essd-11-1017-2019

Sohn, B.-J., Smith, E.A., Robertson, F.R. & Park, S.-C. (2004) Derived over-ocean water vapor transports from satellite-retrieved e–p datasets. *Journal of Climate*, 17(6), 1352–1365. Available from: https://doi.org/10.1175/1520-0442(2004)017⟨1352:DOWVTF⟩2.0.CO;2

Truong, N.M. & Tuan, B.M. (2018) Large-scale patterns and possible mechanisms of 10-20-day intra-seasonal oscillation of the observed rainfall in Vietnam. *International Journal of Climatology*, 38(10), 3801–3821. Available from: https://doi.org/10.1002/joc.5534

Truong, N.M. & Tuan, B.M. (2019) Structures and mechanisms of 20–60-day intraseasonal oscillation of the observed rainfall in Vietnam. *Journal of Climate*, 32(16), 5191–5212. Available from: https://doi.org/10.1175/jcli-d-18-0239.1

Tuan, B.M. (2019) Extratropical forcing of submonthly variations of rainfall in Vietnam. *Journal of Climate*, 32(8), 2329–2348. Available from: https://doi.org/10.1175/jcli-d-18-0453.1

Wu, P., Fukutomi, Y. & Matsumoto, J. (2012) The impact of intraseasonal oscillations in the tropical atmosphere on the formation of extreme central Vietnam precipitation. *Scientific Online Letters on the Atmosphere*, 8, 57–60. Available from: https://doi.org/10.2151/sola.2012-015

Yatagai, A., Kamiguchi, K., Arakawa, O., Hamada, A., Yasutomi, N. & Kitoh, A. (2012) APHRODITE: constructing a long-term daily gridded precipitation dataset for asia based on a dense network of rain gauges. *Bulletin of the American Meteorological Society*, 93(9), 1401–1415. Available from: https://doi.org/10.1175/bams-d-11-00122.1

Yokoi, S. & Matsumoto, J. (2008) Collaborative effects of cold surge and tropical depression-type disturbance on heavy rainfall in central Vietnam. *Monthly Weather Review*, 136(9), 3275–3287. Available from: https://doi.org/10.1175/2008mwr2456.1

Yokoi, S. & Satomura, T. (2005) An observational study of intraseasonal variations over southeast Asia during the 1998 rainy season. *Monthly Weather Review*, 133(7), 2091–2104. Available from: https://doi.org/10.1175/mwr2967.1

Yokoi, S., Satomura, T. & Matsumoto, J. (2007) Climatological characteristics of the intraseasonal variation of precipitation over the indochina peninsula. *Journal of Climate*, 20(21), 5301–5315. Available from: https://doi.org/10.1175/2007jcli1357.1

How to cite this article: Le, H.-H., Hall, N. M. J., & Ngo-Duc, T. (2024). Remote influence on regional scale intraseasonal rainfall variability over Vietnam. *International Journal of Climatology*, *44*(4), 1171–1189. https://doi.org/10.1002/joc.8377